

## Local Optical Properties, Electron Densities, and London Dispersion Energies of Atomically Structured Grain Boundaries

Klaus van Benthem,<sup>1,\*</sup> Guolong Tan,<sup>2</sup> Linda K. DeNoyer,<sup>3</sup> Roger H. French,<sup>2,4</sup> and Manfred Rühle<sup>1</sup>

<sup>1</sup>Max-Planck-Institut für Metallforschung, Heisenbergstrasse 3, 70569 Stuttgart, Germany

<sup>2</sup>Materials Science Department, University of Pennsylvania, 3231 Walnut Street, Philadelphia, Pennsylvania 19104, USA

<sup>3</sup>Deconvolution and Entropy Consulting, 755 Snyder Hill, Ithaca, New York 14850, USA

<sup>4</sup>DuPont Company, Central Research, E356-384, Experimental Station, Wilmington, Delaware 19880, USA

(Received 24 May 2004; published 22 November 2004)

Quantitative analysis of spatially resolved valence electron energy-loss spectra shows strong physical property contrasts for  $\Sigma 5$  and near  $\Sigma 13$  grain boundaries in Fe-doped SrTiO<sub>3</sub>, resulting in London dispersion interaction energies of 14 to 50 mJ/m<sup>2</sup> between the adjacent grains. The determination of local physical properties of grain boundary cores and the appreciable contribution of long-range London dispersion to interface energies provides new information on formation and control of interfaces in materials.

DOI: 10.1103/PhysRevLett.93.227201

PACS numbers: 75.70.Cn, 78.20.Ls, 82.80.Pv

The performance of electronic, optical, and electro-optical devices depends strongly on the properties of the materials of which they are made [1–5]. Often these materials are polycrystalline with properties determined predominantly by the grain boundaries (GBs) [5], exhibiting disordered boundary cores or even amorphous intergranular films. Compared to the adjacent bulk material, GBs often have different chemical compositions and atomic and electronic structures [6–10]. These variations strongly influence the macroscopic materials properties and are responsible for the range of different behaviors in, for instance, functional ceramics. Therefore, a detailed understanding of the atomic and electronic structures of interfaces and, hence, a control over their influence on the overall materials properties is essential for the design of new devices. The study of interfaces in polycrystalline ceramics has heretofore focused on the atomic structure and relative composition changes at the interface, and has relied on a broad characterization of structured grain boundaries as one extreme and intergranular films as the other. We examine interfacial physical property variations across atomically structured grain boundaries and show that atomically structured grain boundaries exhibit local physical properties which distinguish them from bulk phases. It will be shown that these property gradients represent the fundamental basis for appreciable dispersion interactions at the investigated grain boundaries.

We demonstrate that optical properties of atomically structured GBs can be significantly altered locally by structural and chemical changes in the nanometer or subnanometer regime. Interfacial electronic structure data, represented as the local optical properties arising from valence to conduction band transitions, are analyzed and discussed for a  $\Sigma = 5$  (310)  $\theta = 36.87^\circ$  GB and a near  $\Sigma = 13$  (510)  $\theta = 23.6^\circ$  GB in Fe-doped SrTiO<sub>3</sub>. The tilt angle of the near  $\Sigma 13$  boundary ( $n\Sigma 13$ ) is off by  $1^\circ$  from an exact  $\Sigma = 13$  misorientation (i.e.,  $\theta =$

$22.62^\circ$ ), resulting in a core of 0.6 to 0.9 nm width perpendicular to the interface plane [7]. High resolution transmission electron microscopy (HRTEM) micrographs taken from both grain boundary structures are shown in Fig. 1. With the electron beam parallel to the  $\langle 100 \rangle$  direction in bulk SrTiO<sub>3</sub>, both GBs show atomically structured interfaces. The  $\Sigma 5$  grain boundary [Fig. 1(a)] consists of structural units with a short periodicity along the interface plane [7–11]. The  $n\Sigma 13$  GB [Fig. 1(b)] is abrupt with different facets appearing to each side of the boundary plane and a larger structural periodicity length [7]. Although the electronic structure of these grain boundaries has been investigated previously [12,13], no comments concerning local changes of optical properties and electron densities are reported. For an analysis of the interfacial electronic structure, spatially resolved valence electron energy-loss spectroscopy (VEELS) data are compared to data obtained from the bulk SrTiO<sub>3</sub> grains. One hundred single spectra were acquired for energy losses up to 90 eV within line scans across the grain boundaries with lengths varying between 12.5 and 40 nm, corresponding to a spatial separation of adjacent

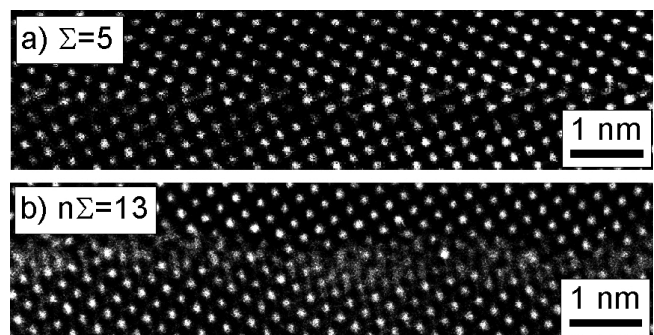


FIG. 1. HRTEM images of (a) the  $\Sigma 5$  (310) and (b) the near  $\Sigma 13$  (510) grain boundaries in SrTiO<sub>3</sub>.

spectra between 0.125 and 0.4 nm. The experimental spectra were corrected for detector dark currents and channel-to-channel gain variations [14]. Multiple scattering effects in the spectra were corrected and the zero-loss peak, fitted by an asymmetrical PearsonVII function [12,15], was removed using Fourier log deconvolution. The resulting single-scattering energy-loss function  $\text{ELF}(E)$  is proportional to  $\text{Im}[-1/\varepsilon(E)]$ , where  $E$  is the measured energy loss and  $\varepsilon(E)$  is the complex dielectric function [15]. Details for the VEELS acquisitions and analysis are published elsewhere [12,15]. The bulk ELF was scaled through application of the index sum rule [16], using  $n = 2.37$  for the index of refraction in bulk  $\text{SrTiO}_3$ , as determined by spectroscopic ellipsometry [17]. Once the quantitative single-scattering ELFs were determined, the Kramers-Kronig relation shown in Eq. (1) was applied to determine  $\text{Re}[-1/\varepsilon(E)]$  [16]:

$$\text{Re}\left(\frac{1}{\varepsilon(E)}\right) = 1 - \frac{2}{\pi} P \int_0^\infty \text{Im}\left(\frac{-1}{\varepsilon(E')}\right) \frac{E'}{E'^2 - E^2} d(E'). \quad (1)$$

Using this Kramers-Kronig analysis, the complex dielectric function  $\varepsilon(E)$  is extracted as a function of energy and position. Hence, any of the conjugate optical properties can quantitatively be determined locally for every position covered by the acquired VEELS line scan.

Figure 2 shows the quantitative index of refraction  $n$  as a function of relative distance to the grain boundary cores. Inside the grains, the index of refraction has values of 2.3 to 2.5, which is comparable to the bulk value. When approaching the boundary cores, the index decreases to values of  $1.56 \pm 0.05$  and  $1.29 \pm 0.05$  for the  $\Sigma 5$  and the  $n\Sigma 13$  interfaces, respectively [18]. Both data sets show asymmetric changes across the boundary cores, which is attributed to spatial drift during data acquisition. Changes in optical properties within the grain boundary cores are

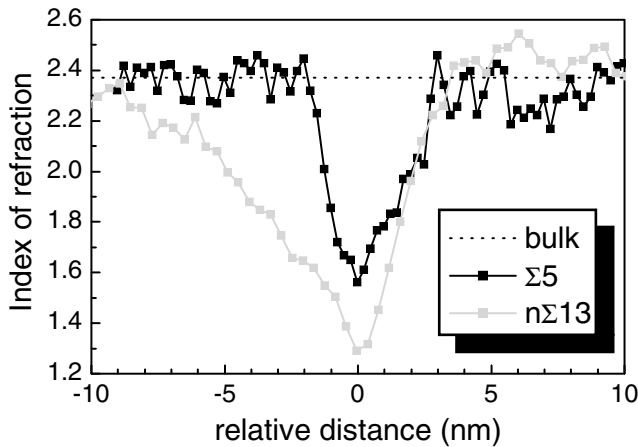


FIG. 2. Local index of refraction across the  $\Sigma 5$  and the  $n\Sigma 13$  grain boundaries. The dashed line marks a value of  $n = 2.37$  for bulk  $\text{SrTiO}_3$  [14]. Error bars are  $\pm 0.05$ .

correlated with changes in the physical density of the materials, the materials high frequency electronic structure, and the polarizability. For these grain boundaries, the mass density of the  $\Sigma 5$  GB core goes down to 39% of the bulk density within roughly  $\pm 1$  nm, while the density at the  $n\Sigma 13$  boundary reduces to 21% of the bulk density of  $\text{SrTiO}_3$  within about  $\pm 2$  nm.

To determine the number of valence electrons which have undergone interband transitions, the oscillator strength or  $f$ -sum rule was applied for energies up to 90 eV [15],

$$N(E) = \frac{m_0}{2\pi^2 \hbar^2 e^2} \int_0^E E' \varepsilon_2(E') dE'. \quad (2)$$

The resulting valence electron densities, reported in units of  $e^-/\text{nm}^3$ , are plotted as a function of transition energy in Fig. 3 for bulk  $\text{SrTiO}_3$  in comparison to the  $\Sigma 5$  and  $n\Sigma 13$  grain boundary cores. The electron density drops from  $558 \pm 7e^-/\text{nm}^3$ , as seen for bulk  $\text{SrTiO}_3$ , to a value of  $428 \pm 7e^-/\text{nm}^3$  present at the  $\Sigma 5$  GB, each evaluated at 90 eV. At  $n\Sigma 13$ , the valence electron density is further reduced to  $234 \pm 7e^-/\text{nm}^3$ . At the  $n\Sigma 13$  GB, the electron density reduction in the boundary cores is associated with the reduced physical density caused by oxygen vacancy formation [10,12,19], which is supported by HRTEM results revealing oxygen vacancies in the core structures of the  $\Sigma = 3$  grain boundaries in  $\text{SrTiO}_3$  [20] and  $\text{BaTiO}_3$  [6]. However, prior structural studies were not quantitative in absolute terms and report relative changes in structure as opposed to density and absolute (volumetric) concentrations. In this study it was possible to directly measure local valence electron densities at GBs quantitatively in the subnanometer regime.

The significant decrease in the local index of refraction and valence electron density in the grain boundary core compared to the bulk demonstrate the presence of strong

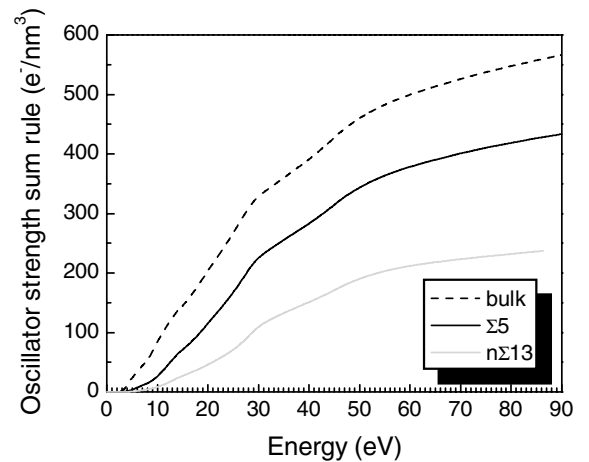


FIG. 3. Valence electron density for bulk  $\text{SrTiO}_3$ , as well as the  $\Sigma 5$  and the  $n\Sigma 13$  grain boundary layers. Error bars are  $\pm 7e^-/\text{nm}^3$ .

optical property gradients (see Figs. 2 and 3). Because of the presence of these gradients, which are the fundamental basis of the long-range London dispersion interaction [16], it is germane to address the magnitude of the London dispersion forces ( $F_{\text{London}}$ ) and interaction energies ( $E_{\text{London}}$ ) to determine their role in interface formation and energy. The nonretarded Hamaker constant,  $A_{121}^{\text{NR}}$ , determines the magnitude of the London dispersion forces between the two adjacent grains (material 1) separated by the grain boundary core (material 2) of width  $L$ , in the nonretarded limit of small interlayer thickness:

$$A_{121}^{\text{NR}} = -6\pi L^3 F_{\text{London}} = -12\pi L^2 E_{\text{London}}. \quad (3)$$

Full spectral Hamaker constants and London dispersion energies shown in Table I were determined based on this three-layer model applying first principles quantum electrodynamic Lifshitz theory [21,22] to the VEELS data [16]. The positive value of  $A_{121}^{\text{NR}}$  constants reveals the existence of attractive London dispersion forces across the grain boundaries with the boundary core serving as an *interfacial layer* of a unique material between the grains. The limiting values for the Hamaker constant are a maximum for a vacuum interlayer and zero if the interfacial layer were indistinguishable from the bulk. Since the optical contrast for the n $\Sigma$ 13 GB is bigger than that of  $\Sigma$ 5, its London dispersion force is larger.

The n $\Sigma$ 13 GB exhibits a larger London dispersion interaction than that reported for grain boundaries with intergranular films in, e.g.,  $\text{Si}_3\text{N}_4$  ceramics [23]. Other comparative examples are colloidal  $\text{SiO}_2$  particles, which exhibit smaller dispersion forces than observed here. The grain boundary London dispersion interactions reported here are appreciable, and, therefore, play an important role in the energetics of GB formation.

For more complex grain boundary structures the usual three-layer model for the dispersion interaction is no longer suitable since properties vary continuously across the GBs. Therefore, we established a new multilayer

model for calculating retarded Hamaker coefficients for graded interfaces based on the approach of Podgornik *et al.* [24]. The Lifshitz formalism with a full spectral approach for retarded Hamaker constants ( $A_{121}^{\text{R}}$ ) is applied, considering the transit time of the electromagnetic fluctuations arising from the finite speed of light [16]. Thus, we can more realistically model the  $\Sigma$ 5 and n $\Sigma$ 13  $\text{SrTiO}_3$  grain boundary structures using the maximal core width perpendicular to the boundary plane of 0.6 [10] and 0.9 nm [7], respectively. A region adjacent to the boundary core was chosen, in which a double-quadratic gradient of the complex optical properties serves as a continuous transition between the bulk and the boundary core, with a thickness of  $d_0 = 0.195$  nm, corresponding to a Ti-O bond length in  $\text{SrTiO}_3$ . Local properties were scaled on the basis of a double-quadratic function as sketched in the right column in Table I. This ensures a continuous scaling of the dielectric function and its first derivative when approaching the GB core from either of the two adjacent grains. Resulting Hamaker coefficient and London dispersion interaction energies for the given core thickness are listed underneath. London dispersion interaction energies are 169 and 119  $\text{mJ/m}^2$  for the three-layer and the multilayer models, respectively, if the boundary core is essentially vacuum. These energies are appreciable and of the order of 10% of surface energies for  $\text{SrTiO}_3$  [25]. The graded-interface model leads to only a small reduction in the calculated magnitude of the London dispersion interaction at the investigated  $\text{SrTiO}_3$  grain boundaries. The important role of the dispersion interaction in grain boundary formation and the final equilibrium GB structure can be seen from the large changes in the dispersion energy comparing the free surface and the grain boundary. Forming the n $\Sigma$ 13 GB regains about 69  $\text{mJ/m}^2$  (i.e., 58%) of London dispersion energy in the GB structure (compared to 119  $\text{mJ/m}^2$ ). The  $\Sigma$ 5 GB regains about 105  $\text{mJ/m}^2$ , corresponding to about 88% of the London dispersion energy of the free surfaces.

TABLE I. Calculated nonretarded ( $A_{121}^{\text{NR}}$ ) and retarded ( $A_{121}^{\text{R}}$ ) Hamaker constants for the abrupt gradient and double-quadratic gradient models, respectively.  $d_0$  is the gradient thickness. Retarded Hamaker coefficients are evaluated for a central layer thickness of  $L = 0.9$  (n $\Sigma$ 13) and  $L = 0.6$  nm ( $\Sigma$ 5). Dispersion energies are evaluated setting  $L$  equal to  $d_0$ . Relative errors are 3%.

| Interface   | Abrupt gradient                       |  | Double-quadratic gradient            |  |
|---|---------------------------------------|--|--------------------------------------|--|
|   | $A_{121}^{\text{NR}}$ ( $\text{zJ}$ ) | $E_{\text{London}}$ ( $\text{mJ m}^{-2}$ ) | $A_{121}^{\text{R}}$ ( $\text{zJ}$ ) | $E_{\text{London}}$ ( $\text{mJ m}^{-2}$ ) |
| $\text{SrTiO}_3 \text{vac} \text{SrTiO}_3$<br>$d_0 = 0.195$ nm        | 243.9                                 | 169  | 171.2<br>( $L = 0.9$ nm)             | 119  |
| $\text{SrTiO}_3 \text{n}\Sigma 13 \text{SrTiO}_3$<br>$d_0 = 0.195$ nm | 105.5                                 | 73   | 72.5<br>( $L = 0.9$ nm)              | 50   |
| $\text{SrTiO}_3 \Sigma 5 \text{SrTiO}_3$<br>$d_0 = 0.195$ nm          | 35.0                                  | 24   | 20.7<br>( $L = 0.6$ nm)              | 14   |
| $\text{SiO}_2 \text{vac} \text{SiO}_2$<br>$d_0 = 0.165$ nm            | 68.2                                  | 66   | 50.3                                 | 49   |

Although London dispersion energies of 14–24 mJ/m<sup>2</sup> and 50–73 mJ/m<sup>2</sup> for the two investigated grain boundaries are small, they represent appreciable amounts of roughly 4%–10% of the total grain boundary energies. Dispersion forces have usually been considered in multiphase systems. Here we show that a GB can be considered as just such a *multiphase* system through changes in materials properties on the atomic level. Dispersion forces present at low-energy grain boundaries contribute to the interface energies and are directly and quantitatively measurable by spatially resolved VEELS experiments. Theoretical calculations so far do not account for long-range London dispersion interactions, caused by the exchange of virtual photons between the two crystals across the grain boundary cores. It is, however, surprising that these effects appreciably contribute by up to 10% to the GB energy, which to date was thought to be determined by interatomic bonding only.

Previous studies did not address quantitative changes in the physical properties of the core, even though these can drive structural changes. Grain boundary formation is the result of numerous interactions, such as chemical composition, bonding interactions, electrostatic interactions, London dispersion, and dipolar interactions, i.e., Keesom and Debye. The thermodynamics and kinetics of GB formation are dependent on all of these interactions. Many times, if close to an equilibrium structure, dispersion forces can play a dominant role, whereas in the formation process chemical interactions may initially have dominated. It is therefore essential to quantitatively consider all of the fundamental interactions at play. Our quantitative determination of the spatially resolved complex optical properties and valence electron densities for these boundaries represents new information not previously available for these important microstructural features. In addition, the presence and role of long-range London dispersion interactions at atomically structured grain boundaries or interfaces have not been previously demonstrated. The current results show that the London dispersion energies represent an appreciable contribution of up to 10% to the total grain boundary energy. Their role in determining the final microstructure and properties of grain boundaries in functional materials is now accessible for future studies. The determination of quantitative physical properties and interfacial electronic structure of grain boundaries at high spatial resolution go beyond previous interface studies that focused on atomic structural or compositional observations of interfaces. A combination of this technique with well established routes for atomic structure and composition analyses gives a deeper fundamental understanding of formation processes, how certain grain boundary structures and microstructures are established, and how to optimize these to produce novel functional materials with desirable properties and performance.

This work is partially supported by the EU under Contract No. G5RD-CT-2001-00586 and by NSF Grant No. DMR-0010062. The authors acknowledge helpful discussions with V. A. Parsegian and editorial comments of B. B. French.

---

\*Present address: Oak Ridge National Laboratory, One Bethel Valley Road, Oak Ridge, TN 37831-6031, USA.

- [1] M. Verkerk, B. J. Middelhuys, and A. J. Burggraaf, *Solid State Ionics* **6**, 159 (1982).
- [2] R. Gerhardt and A. S. Nowick, *J. Am. Ceram. Soc.* **69**, 641 (1986).
- [3] I. Denk *et al.*, *Ber. Bunsen-Ges. Phys. Chem.* **99**, 798 (1995).
- [4] R. Waser, in *Proceedings of the Third Euro-Ceramics*, edited by P. Duran and J. F. Fernandez (Faenza Editrice Iberica, Castellon de la Plana, Spain, 1993), Vol. 23.
- [5] Y. M. Chiang, D. P. Birnie III, and W. D. Kingery, *Physical Ceramics* (John Wiley & Sons, New York, 1997).
- [6] C. L. Jia and K. Urban, *Science* **303**, 2001 (2004).
- [7] S. Hutt, O. Kienzle, F. Ernst, and M. Rühle, *Z. Metallkd.* **92**, 105 (2001).
- [8] O. Kienzle, M. Exner, and F. Ernst, *Phys. Status Solidi A* **166**, 75 (1998).
- [9] F. Ernst, O. Kienzle, and M. Rühle, *J. Eur. Ceram. Soc.* **19**, 665 (1999).
- [10] N. D. Browning and S. J. Pennycook, *J. Phys. D* **29**, 1779 (1996).
- [11] D. A. Bonnell, *J. Am. Ceram. Soc.* **81**, 3049 (1998).
- [12] K. van Benthem *et al.*, *Ultramicroscopy* **86**, 303 (2001).
- [13] D. A. Bonnell and S. V. Kalinin, *Solid State Phenomena* **80–81**, 33 (2001).
- [14] R. F. Egerton, *Electron Energy Loss Spectroscopy in the Electron Microscope* (Plenum Press, New York and London, 1996).
- [15] A. D. Dorneich *et al.*, *J. Microsc.* **191**, 286 (1998).
- [16] R. H. French, *J. Am. Ceram. Soc.* **83**, 2117 (2000).
- [17] K. van Benthem, C. Elsässer, and R. H. French, *J. Appl. Phys.* **90**, 6156 (2001).
- [18] Very low beam currents of the order of a few pA were used for data acquisition, so that the specimen is hit by one beam electron every 10<sup>-7</sup> to 10<sup>-8</sup> s. Provided each beam electron generates one electron-hole pair with a lifetime of about 10<sup>-15</sup> s, subsequent beam electrons do not suffer from any recombination characteristics.
- [19] N. D. Browning *et al.*, *Appl. Phys. Lett.* **74**, 2638 (1999).
- [20] Z. Zhang *et al.*, *Science* **302**, 846 (2003).
- [21] E. M. Lifshitz, *Sov. Phys. JETP* **2**, 73 (1956).
- [22] I. E. Dzyaloshinskii, E. M. Lifshitz, and L. P. Pitaevskii, *Adv. Phys.* **10**, 165 (1961).
- [23] R. H. French *et al.*, *Acta Mater.* **46**, 2271 (1998).
- [24] R. Podgornik, P. L. Hansen, and V. A. Parsegian, *J. Chem. Phys.* **119**, 1070 (2003).
- [25] J. Padilla and D. Vanderbilt, *Surf. Sci.* **418**, 64 (1998).